CHEMISTRY OF MATERIALS
Article

Chem. Mater. **2010,** *22,* 3693–3697 3693
DOI:10.1021/cm100487j

X-ray Microscopy Imaging of the Grain Orientation in a Pentacene Field-Effect Transistor

Björn Bräuer,*,† Ajay Virkar,‡ Stefan C. B. Mannsfeld,§ David P. Bernstein,† Roopali Kukreja,⊥ Kang Wei Chou,∥ Tolek Tyliszczak,∥ Zhenan Bao,*,‡ and Yves Acremann⊥

†*SIMES Center, SLAC National Accelerator Laboratory,* ‡*Department of Chemical Engineering, and* ⊥*PULSE Center, SLAC National Accelerator Laboratory, Stanford University, Stanford, California 94309,* §*SSRL, SLAC National Accelerator Laboratory, Stanford, California 94309, and* ∥*Advanced Light Source, Berkeley, California 94720*

Received February 16, 2010. Revised Manuscript Received April 16, 2010

We demonstrate the application of scanning transmission X-ray microscopy (STXM) to image the angular distribution of grains in organic semiconductor thin film devices on the example of pentacene field-effect transistors. The in-plane orientation of the molecules in the channel region and underneath the top conducting electrodes was derived from polarization dependent STXM investigations. The method allows the determination of the actual grain size and the correlation of the electronic transport and structural properties on the nanometer length scale.

Introduction

Organic field-effect transistors (OFETs) are attracting attention due to their potential application in cheap, flexible, and large-area electronic devices. Field-effect mobilities of up to 5 $cm^2/(V\ s)$ have been reported for pentacene.[1−3] The structural quality of organic semiconductors was shown to be the key parameter for achieving high field-effect mobility values.[4] For example, a mobility of 35 $cm^2/(V\ s)$ was reported for a pentacene single crystal at room temperature.[5] Polycrystalline films are composed of grains and grain boundaries. Hopping type transport is limited in such films due to significant charge-carrier trapping at the grain boundaries.[6−13] Detailed structural information about pentacene-based thin films can be obtained by X-ray diffraction.[14] Pentacene consists of five aromatic linearly fused rings with two molecules per unit cell. In thin films, the neighboring molecules form a herringbone pattern enclosing a herringbone angle of 53°.[14] The long axes of the molecules are oriented in parallel relative to the substrate normal (0°),[14,15] and are more tilted toward the substrate plane (6°) for thicker films (20 nm).[16−20] The growth of pentacene on silicon was successfully imaged by photoemission electron microscopy (PEEM);[21] however, the orientation of molecules within discrete grains was not clearly evident. Additional information about the grain morphology and orientation of ultrathin (2 nm) crystalline organic films can be obtained by transverse shear microscopy.[22] This technique can only be applied to visualize the

*Corresponding authors. Phone: 650 926 2996. Fax: 650 926 4100. E-mail: bbj@stanford.edu (B.B.). Phone: 650 723 2419. Fax: 650 723 9780. E-mail: zbao@stanford.edu (Z.B.).

(1) Gelinck, G. H.; Huitema, H. E. A.; Veenendaal, E.; Cantatore, E.; Schrijnemakers, L.; Putten, J. B. P. H.; Geuns, T. C. T.; Beenhakkers, M.; Giesbers, J. B.; Huisman, B.-H.; Meijer, E. J.; Benito, E. M.; Touwslager, F. J.; Marsman, A. W.; Rens, B. J. E.; Leeuw, D. M. *Nat. Mater.* **2004**, *3*, 106.
(2) Baude, P. F.; Ender, D. A.; Haase, M. A.; Kelley, T. W.; Muyres, D. V.; Theiss, S. D. *Appl. Phys. Lett.* **2003**, *82*, 3964.
(3) Kelley, T. W.; Muyres, D. V.; Baude, P. F.; Smith, T. P.; Jones, T. D. *Mater. Res. Soc. Symp. Proc.* **2003**, *771*, L.6.5.1.
(4) Bao, Z.; Lovinger, A.; Dodabalpur, A. *Adv. Mater.* **1997**, *9*, 42.
(5) Jurchescu, O. D.; Popincius, M.; Wees, B. J.; Palstra, T. T. M. *Adv. Mater.* **2007**, *19*, 688.
(6) Nelson, S. F.; Lin, Y.-Y.; Gundlach, D. J.; Jackson, T. N. *Appl. Phys. Lett.* **1998**, *72*, 1854.
(7) Horowitz, G.; Hajlaoui, M. E. *Adv. Mater.* **2000**, *12*, 1046.
(8) Kelley, T. W.; Frisbie, C. D. *J. Phys. Chem. B* **2001**, *105*, 4538.
(9) Someya, T.; Katz, H. E.; Gelperin, A.; Lovinger, A. J.; Dodabalapur, A. *Appl. Phys. Lett.* **2002**, *81*, 3079.
(10) Di Carlo, A.; Piacenza, F.; Bolognesi, A.; Stadlober, B.; Maresch, H. *Appl. Phys. Lett.* **2005**, *86*, 263501.
(11) Zhang, J.; Rabe, J. P.; Koch, N. *Adv. Mater.* **2008**, *20*, 3254.
(12) (a) Bräuer, B.; Vaynzof, Y.; Zhao, W.; Kahn, A.; Li, W.; Zahn, D. R. T.; Fernández, C. J.; Sangregorio, C.; Salvan, G. *J. Phys. Chem. B* **2009**, *113*, 4565. (b) Bräuer, B.; Grobosch, M.; Knupfer, M.; Weigend, F.; Vaynzof, Y.; Kahn, A.; Rüffer, T.; Salvan, G. *J. Phys. Chem. Lett.* **2009**, *113*, 10051. (c) Bräuer, B.; Zahn, D. R. T.; Rüffer, T.; Salvan, G. *Chem. Phys. Lett.* **2006**, *432*, 226.
(13) (a) Bräuer, B.; Fronk, M.; Lehmann, D.; Zahn, D. R. T.; Salvan, G. *J. Phys. Chem. B* **2009**, *113*, 14957. (b) Fronk, M.; Bräuer, B.; Kortus, J.; Schmidt, O. G.; Zahn, D. R. T.; Salvan, G. *Phys. Rev. B* **2009**, *79*, 235305.
(14) Mannsfeld, S. C. B.; Virkar, A.; Reese, C.; Toney, M. F.; Bao, Z. *Adv. Mater.* **2009**, *21*, 2294.
(15) Mattheus, C.; Dros, A.; Baas, J.; Meetsma, A.; Boer, J.; Palstra, T. *Acta Crystallogr Sect. C* **2001**, *57*, 939.
(16) Schiefer, S.; Huth, M.; Dobrinevski, A.; Nickel, B. *J. Am. Chem. Soc.* **2007**, *129*, 10316.
(17) Dimitrakopoulos, C. D.; Brown, A. R.; Pomp, A. *Appl. Phys.* **1996**, *80*, 2501.
(18) Ruiz, R.; et al. *Appl. Phys. Lett.* **2004**, *85*, 4926.
(19) Fritz, S.; Martin, S.; Frisbie, C.; Ward, M.; Toney, M. *J. Am. Chem. Soc.* **2004**, *126*, 4084.
(20) Mayer, A. C.; Kazimirov, A.; Malliaras, G. G. *Phys. Rev. Lett.* **2006**, *97*, 105503.
(21) Meyer, zu; Heringsdorf, F. J.; Reuter, M. C.; Tromp, R. M. *Nature* **2001**, *412*, 517.
(22) Kalihari, V.; Tadmor, E. B.; Haugstad, G.; Frisbie, C. D. *Adv. Mater.* **2008**, *20*, 4033.

Published on Web 05/19/2010

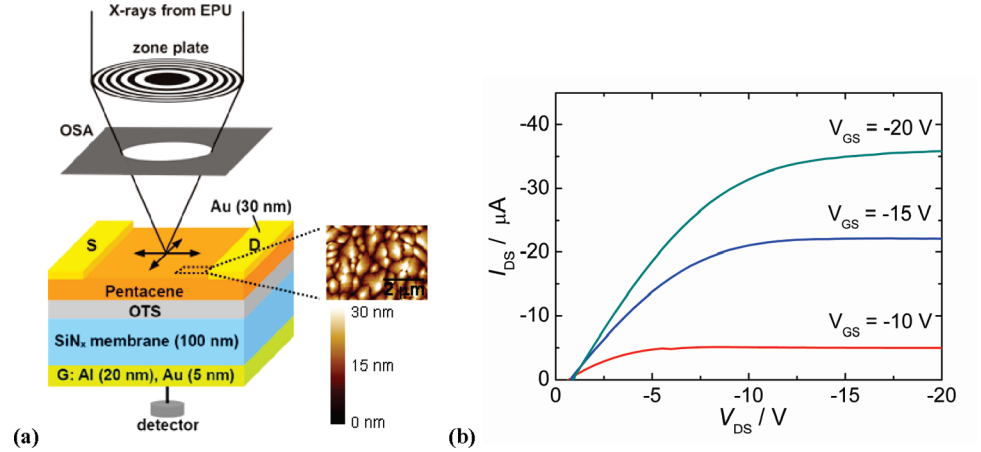

Figure 1. (a) Schematic of the pentacene-based OFET raster scanned by X-rays. The X-ray beam comes from an EPU and is focused through a zone plate and an order sorting aperture (OSA). The atomic force microscopy (AFM) image on the right side shows the topography of pentacene. (b) I_{DS} vs V_{DS} characteristic of the prepared pentacene OFET. The measurements were carried out in ambient atmosphere (1 h after the device was exposed to an ambient environment).

microstructure in smooth, elastically compliant, and anisotropic crystalline films.

In this work, scanning transmission X-ray microscopy (STXM) will be introduced as a complementary method to obtain orientational information about the molecules in bulk structures, which is of importance for organic solar cells and field-effect transistors. In STXM, the X-ray beam coming from an elliptically polarized undulator (EPU) beamline is focused by a zone plate to provide a lateral resolution of 30 nm.[23,24] The sample is then raster scanned relative to the X-ray beam while the transmitted photon flux is detected. The imaging method is becoming increasingly popular owing to the following advantages: the relatively low radiation damage, the compositional information that is provided by near-edge X-ray absorption fine-structure spectroscopy (NEXAFS),[25,26] the ability to image buried layers underneath several tens of nanometer thin films,[27] and its sensitivity to the molecular orientation due to the linear dichroism effect.[13,30−37] The usefulness of the technique for studying the morphology and composition of organic photovoltaic devices has been shown in the literature.[28−30] Moreover, an EPU can produce X-rays of any linear and circular polarization at variable wavelengths. The polarization angle of the linearly polarized X-rays will be varied for studying the in-plane orientation of pentacene molecules within the grains of an OFET. A SiN_x membrane (100 nm thick) was used as the substrate for our STXM investigations as it has a low X-ray absorption cross section. At the same time, the membrane was used as the gate dielectric layer in our pentacene-based OFETs. A schematic of such an OFET is shown in Figure 1a.

Experimental Section

The membranes for the OFET were prepared at the Stanford Nanofabrication Facility. The membrane surface was rinsed with acetone and isopropyl alcohol and treated with UV ozone for about 20 min. Octadecyltrichlorsilane (OTS) was used to modify the surface of the membrane. To form the monolayer of OTS, the cleaned membrane substrates were placed in a desiccator with a heated metal block (200 °C). Three to four drops of neat OTS were placed onto the block, and the desiccator was put under vacuum overnight. The substrates were washed with isopropyl alcohol and dried with a nitrogen gun prior to deposition of pentacene. A 30 nm portion of pentacene was subsequently deposited at 60 °C substrate temperature on top of the OTS-treated membrane. A 20 nm thick aluminum film, covered with 5 nm of gold, was deposited on the backside of the membrane functioning as the gate electrode.[37] The source and drain electrodes consist of 40 nm of gold and were deposited on top of the pentacene layer using a shadow mask; the channel width was 1 mm, and channel length was 45 μm. Pentacene was purchased from Aldrich Chemical Co. and was vacuum sublimed once.

STXM measurements were carried out at the elliptical polarizing undulator (EPU) beamline 11.0.2 at the Advanced Light

(23) Kilcoyne, A. L. D.; Tyliszczak, T.; Steele, W. F.; Fakra, S.; Hitchcock, P.; Franck, K.; Anderson, E.; Harteneck, B.; Rightor, E. G.; Mitchell, G. E.; Hitchcock, A. P.; Yang, L.; Warwick, T.; Ade, H. *J. Synchrotron Rad.* **2003**, *10*, 125.
(24) Stöhr, J.; Siegmann, H. C. *Magnetism*; Springer-Verlag: Berlin, Heidelberg, 2006.
(25) (a) Ade, H.; Stoll, H. *Nat. Mater.* **2009**, *8*, 281. (b) Ade, H.; Hitchcock, A. P. *Polymer* **2008**, *49*, 643–675.
(26) McNeill, C. R.; et al. *Macromolecules* **2007**, *40*, 3263–3270. (b) McNeill, C. R.; et al. *Nanotechnology* **2008**, *19*, 424015.
(27) Acremann, Y.; Strachan, J. P.; Chembrolu, V.; Andrews, S. D.; Tyliszczak, T.; Katine, J. A.; Carey, M. J.; Clemens, B. M.; Siegmann, H. C.; Stöhr, J. *Phys. Rev. Lett.* **2006**, *96*, 217202.
(28) Burke, K. B.; et al. *Macromolecules* **2009**, *42*, 3098.
(29) Kaznacheev, K.; Hegmann, T. *Phys. Chem. Chem. Phys.* **2007**, *9*, 1705.
(30) Urquhart, S. G.; Lanke, U. D.; Fu, J. *Int. J. Nanotechnol.* **2008**, *5*, 1138.
(31) Ade, H.; Hsiao, B. *Science* **1993**, *262*, 1427.
(32) Smith, A. P.; Ade, H. *Appl. Phys. Lett.* **1996**, *69*, 3833.
(33) Fu, J.; Urquhart, S. G. *Langmuir* **2007**, *23*, 2615.
(34) Hernandez-Cruz, D.; Rousseau, M.; West, M. M.; Pezolet, M.; Hitchcock, A. P. *Biomacromolecules* **2006**, *7*, 836.
(35) Smith, A. P.; Bai, C.; Ade, H.; Spontak, R. J.; Balik, C. M.; Koch, C. C. *Macromol. Rapid Commun.* **1998**, *19*, 557.
(36) (a) Fink, R.; Groh, U.; Meigs, G.; Ade, H. Advanced Light Source Compendium of User Abstracts. **2000**; this is a publication of a national laboratory, available on line at http://www.als.lbl.gov/als/compendium/AbstractManager/uploads/00172.pdf. (b) Fink, R.; Ade, H., Kilcoyne; D., Groh, U.; Schmidt, T.; Umbach, E. Advanced Light Source Compendium of User Abstracts. **2002**; this is a publication of a national laboratory, available on line at http://www.als.lbl.gov/als/compendium/AbstractManager/ uploads/02115.pdf.
(37) Fink, R. H.; Hub, C.; Tzvetkov, G. *Acta Physica Polonica A* **2009**, *115*, 462.

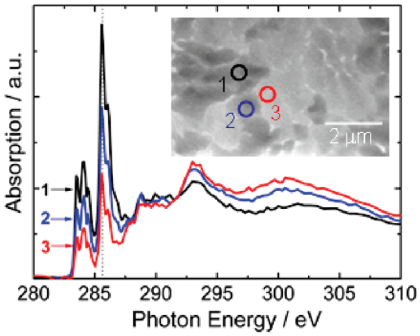

Figure 2. X-ray absorption spectra of pentacene (30 nm). The inset shows a STXM image of a region of a pentacene-based organic field-effect transistor collected at a photon energy of 285.6 eV and 0° polarization. The spectra were recorded for different grains (1, 2, and 3). The areas over which the spectra were averaged are marked by circles. In each of them, the molecules have different orientations leading to different intensities in the NEXAFS spectra. The resonances between 283 and 287 eV correspond to transitions of core electrons in carbon into unoccupied π^* states of the sp^2-hybridized carbon atoms,[38,39] between 287 and 291 eV into C−H*/Rydberg states, and between 291 and 315 eV into σ^* states.[40]

Source (ALS) in Berkeley, California (USA). A photon energy range of 280−320 eV was used for the investigations. The resolution of the zone plate was approximately 35 nm. STXM images were taken at normal incidence. All measurements were performed at room temperature in He atmosphere.

Each image was taken within 5−8 min which means that one molecule is exposed by X-rays for less than 10 ms. Thus the radiation damage is negligibly low and does not influence the experimental results. This was also checked by taking NEXAFS spectra before and after the measurements which did not show any changes.

The electrical measurements on the organic devices were performed under ambient conditions using a Keithley 4200SCS semiconductor parameter analyzer. The atomic force microscope (AFM) images of pentacene thin films were collected using a Digital Instruments MMAFM-2 scanning probe microscope.

Results and Discussion

The typical drain source current (I_{DS}) vs drain source voltage (V_{DS}) characteristic of the OFET structure with a 30 nm pentacene active layer is shown in Figure 1b. Derived from these measurements, the charge carrier mobility is in the range of 0.1 $cm^2/(V\ s)$, similar to those reported in the literature.[1]

The NEXAFS spectra of several single pentacene grains are shown in Figure 2. Three different types of resonances can be assigned to transitions of core electrons in the carbon atoms: transitions into unoccupied π^* states of the sp^2-hybridized carbon atoms between 283 and 287 eV,[38,39] into C−H*/Rydberg states between 287 and 291 eV, and into σ^* states between 291 and 315 eV.[40]

The pentacene molecules in each crystalline grain exhibit highly defined in-plane angles which leads to pronounced differences in the intensity of the π^* resonances for different grains. This effect was used for mapping the orientation distribution of the pentacene grains in the OFET devices in the channel region and underneath the gold electrodes.

Figure 3 shows STXM images, recorded at 285.6 eV, with the respective rotation angles of the electric field vector **E** of the linearly polarized incoming X-rays. The upper dark half of the images shows the pentacene grains underneath the Au electrode. The lower brighter part of the images shows the pentacene grains in the channel region, i.e., without Au on top.

The images show the existence of pentacene grains with sizes ranging from 100 nm to several micrometers similar to what is shown in the AFM images in Figure 1a. The grains are separated from each other by grain boundaries, illustrated by the bright lines corresponding to a low X-ray absorption intensity in Figure 3. The molecular orientation in neighboring segments within a grain is the same forming large areas of uniform molecular orientation. Two of such domains were marked in Figure 3 showing the dependence of the brightness, i.e., the X-ray absorption cross section of differently oriented grains on the rotation angle of the linearly polarized X-rays. The upper grain reveals the highest X-ray absorption at 0° polarization whereas the lower one at 75°, indicating different in-plane orientations of the molecules within these certain domains.

From the polarization dependent measurements, the azimuthal angle $\beta(x,y)$ of the pentacene islands relative to the in-plane X-ray polarization vector has been obtained. The following approach was utilized for the fitting procedure[40] of the absorbance $A(x,y)$ of the sample:

$$A(x,y) = a_0 t(1 + a_1 \cos^2(\beta(x,y) - \delta - \alpha_p) + a_1 \cos^2(\beta(x,y) + \delta - \alpha_p)) \quad (1)$$

where a_0 represents the absorption of the pentacene film with thickness t, a_1, the strength of the linear dichroism effect, and α_p, the X-ray polarization angle. The local angles toward the x axis for the two differently oriented molecules in the unit cell are represented by $\beta(x,y) - \delta$ and $\beta(x,y) + \delta$ where 2δ is approximately 53°.[6] The transmitted intensity is therefore

$$I = I_0 e^{-A(x,y)} \quad (2)$$

with I_0 being the incident intensity. Notice that a_1 is independent of the position x, y on the sample. We can determine the topographic contrast $a_0 t$ from the images with $\alpha_p = 0°$ and $\alpha_p = 90°$ as

$$a_0 t = (A_{0°} + A_{90°})/(2 + a_1) \quad (3)$$

where $A = -\ln(I/I_0)$ for 0 and 90° polarization. After substituting $a_0 t$ in eq 1 by the expression in eq 3, we fit $A(x,y)$ to the experimental data with a_1 being constant and $\beta(x,y)$ being variable for each pixel.

Figure 4a shows the pentacene molecules viewed from the top of the film and explains schematically how the

(38) Stöhr, J.; Gland, J. L.; Kolllin, E. B.; Koestner, P. J.; Johnson, A. L.; Muetterties, E. L.; Sette, F. *Phys. Rev. Lett.* **1984**, *53*, 2161–2164.
(39) Stöhr, J.; Samant, M. G. *J. Electron Spectrosc. Relat. Phenom.* **1999**, *98−99*, 189–207.
(40) Stöhr, J. *NEXAFS Spectroscopy*, first ed.; Springer: New York, 1992.

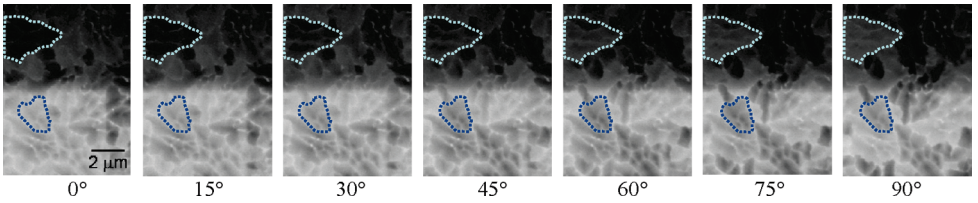

Figure 3. STXM images on a pentacene-based organic field-effect transistor collected at a photon energy of 285.6 eV. Each image has a size of $10 \times 7.5\,\mu m^2$ and was recorded under different orientations α_p (0−90°) of the electric field vector of the incoming linearly polarized X-rays in normal direction to the sample surface. The upper dark half of the images shows the pentacene grains underneath the Au electrode. The lower bright part of the images shows the pentacene grains in the channel region, i.e., without Au on top. Two domains are marked illustrating the dependence of the X-ray absorption intensity on the polarization angle.

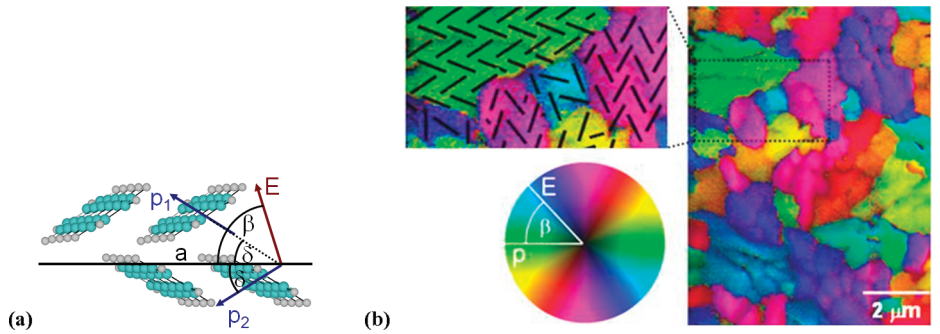

Figure 4. (a) Schematic of the interaction of the electric field vector **E** with the electric transition dipole moments $\mathbf{p}_1$ and $\mathbf{p}_2$ of the π^* orbitals of pentacene. Maximal absorption can be obtained when **E**, and the short unit cell axis "a" are parallel to each other ($\beta = 0$). (b) Distribution of the molecular orientation is given according to the color circle scheme where, green, blue, and red stand for $\beta = 0°$, 60°, and 120°, respectively. The dark contrast reflects the topography, calculated from the STXM images in Figure 3. The black lines in the upper left image represent the C−C bond along the short axis of the pentacene molecule.

molecular orientation of the aromatic system can be derived from STXM measurements. The X-ray absorption $A(x,y)$ reaches its maximum when the electronic transition dipole moment **p** of the molecules is aligned parallel to the electric field **E** of the incoming X-ray ($\beta = 0°$ and 180°). For $\beta = 90°$ and 270°, the interaction between **E** and **p** is minimal. The pentacene unit cell contains two molecules with different **p** vectors $\mathbf{p}_1$ and $\mathbf{p}_2$ that are rotated symmetrically by $\pm\delta$ from the short unit cell axis (neglecting the slight vertical tilt[16−20] of the molecules in the thin film phase; see Figure 4a). Consequently, the direction of the maximum in the X-ray absorption, to which both types of the molecules contribute equally, will coincide with the short unit cell axis. This effect was used for determining the orientation of the pentacene molecules within the grains using eq 1.

Figure 4b shows the topography of the pentacene film, reconstructed from the X-ray absorption intensity, and the molecular orientation, calculated from the STXM images at the same location where the images in Figure 3 were captured. It illustrates the distribution of the molecular orientation with approximately 40 nm lateral resolution. The green color implies that $\beta(x,y)$, the angle between the electric field vector **E** and the short axis of the pentacene unit cell, cf. Figure 4a, is close to zero, blue stands for $\beta(x,y) = 60°$ etc., cf. the colored circle on the left side in Figure 4b. In contrast to Figure 3, the brightness in Figure 4 represents the film thickness. The darker areas in Figure 4 refer to grain boundaries or voids in the film. The grain orientation map shows that the molecular orientation does not change between neighboring grain segments partially consisting of lobes or overgrowths. This leads to a long-range ordered domain structure in agreement with TSM studies on ultrathin pentacene films.[22] Interestingly, the long-range order is preserved in thicker films and the domain size is comparable to what was reported for thin pentacene films.[22]

The meaning of **p** in terms of molecular orientation within the grains is illustrated in the upper left schematic of Figure 4b. From the image, the angle of adjacent grains can be estimated and high and low angle grain boundaries can be distinguished. Conventionally, a grain boundary is low angle when the relative orientation of molecules in adjacent grains is less than 15°; otherwise, it is referred to as high angle.[41] Accordingly, the charge transport between, e.g., yellow and light blue marked grains, should be less efficient than between light blue and violet marked grains.

The statistical distribution of the grain orientation in the channel region of the pentacene field effect transistor is shown in Figure 5a. The analysis was performed in a $10 \times 10\,\mu m^2$ large area. It can be seen that there is no preferential orientation of the grains on the substrate and the number of grains with a certain orientation is almost the same for all the angles. This is expected since the grains start to grow separately with a random orientation on the substrate during the vacuum deposition process and no preferential orientation was forced in the experiment. In general, the larger the scanned areas

(41) Flewitt, P. E. J.; Wild, R. K. *Grain Boundaries: Their Microstructure and Chemistry*; Wiley: New York, 2001.

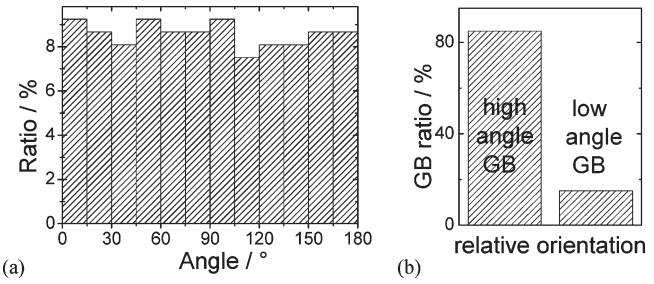

Figure 5. Histograms showing (a) the distribution of the different grain orientations and (b) the ratio of high and low angle grain boundaries (GB).

the smaller are the deviations in the ratio for the different angles.

As outlined in the previous paragraph, the orientation of the molecules in adjacent grains is of great importance for the performance of transistor devices. The statistical distribution in Figure 5b was calculated by determining the molecular orientation in one grain and comparing this with the angle of the molecules in all adjacent grains. This procedure was repeated for all grains in a $10 \times 10\ \mu m^2$ large area. In average, for no more than 15% of the adjacent grains, an angle of 15° or less was found between the neighboring grains. This means that about 15% of the grain boundaries are so-called low angle and 85% are high angle grain boundaries. This is very similar to the results in literature[22] obtained for very thin films where about 10% were found to be low angle grain boundaries.

This angle is supposed to be dependent on parameters like the substrate temperature and the properties of the interface and will be investigated in more detail in future. Therefore, STXM can be used to probe the relation between microstructure and electric transport in detail when combined with scanning probe techniques which measure the charge density distribution. STXM by itself does not provide enough sensitivity to probe electronic changes when applying a bias voltage (20 V) to our OFET devices.

Summary

We have built up pentacene-based OFET devices on SiN_x membranes. We have shown that the in-plane molecular orientation, which is of prime importance for the performance of organic semiconductor devices, can be derived from STXM measurements and that pentacene consists of 100 nm to several μm large grains consisting of lobes and overgrowths in which the pentacene molecules have a uniform orientation. Compared to TSM which can be applied to ultrathin films[22] the STXM is a bulk sensitive technique and allows, in addition, studying the orientation of molecules buried underneath metal films and has less requirements regarding the surface quality. In future, the structural information will be correlated with electronic properties derived from other scanning probe techniques.

Acknowledgment. B.B. would like to thank the German Research Foundation (DFG) for a postdoctoral fellowship. A.V. and Z.B. thank the NSF sponsored MRSEC (DMR 0213618) and NSF Solid State Chemistry (DMR 0705687) for financial support. The ALS and the research of the SLAC authors is funded by DOE-BES.